MAIN-BELT ASTEROIDS OBSERVED FROM CS3: 2020 OCTOBER TO DECEMBER

Robert D. Stephens
Center for Solar System Studies (CS3) / MoreData!
11355 Mount Johnson Ct., Rancho Cucamonga, CA 91737 USA
rstephens@foxandstephens.com

Brian D. Warner
Center for Solar System Studies (CS3) / MoreData!
Eaton, CO

(Received: 2021 Jan 6)

CCD photometric observations of 12 main-belt asteroids were obtained at the Center for Solar System Studies (CS3) from 2020 October to December.

The Center for Solar System Studies (CS3) has seven telescopes which are normally used in program asteroid family studies. The focus is on near-Earth asteroids, but when suitable targets are not available, Jovian Trojans and Hildas are observed. When a nearly full moon is too close to the family targets being studied, targets of opportunity amongst the main-belt families were selected.

Table I lists the telescopes and CCD cameras that were used to make the observations. Images were unbinned with no filter and had master flats and darks applied. The exposures depended upon various factors including magnitude of the target, sky motion, and Moon illumination.

Telescope	Camera
0.30-m f/6.3 Schmidt-Cass	FLI Microline 1001E
0.35-m f/9.1 Schmidt-Cass	FLI Microline 1001E
0.35-m f/9.1 Schmidt-Cass	FLI Microline 1001E
0.35-m f/9.1 Schmidt-Cass	FLI Microline 1001E
0.35-m f/11 Schmidt-Cass	FLI Microline 1001E
0.40-m f/10 Schmidt-Cass	FLI Proline 1001E
0.50-m F8.1 R-C	FLI Proline 1001E

Table I: List of CS3 telescope/CCD camera combinations.

Image processing, measurement, and period analysis were done using *MPO Canopus* (Bdw Publishing), which incorporates the Fourier analysis algorithm (FALC) developed by Harris (Harris et al., 1989). The Comp Star Selector feature in *MPO Canopus* was used to limit the comparison stars to near solar color. Night-to-night calibration was done using field stars from the ATLAS catalog (Tonry et al., 2018), which has Sloan *griz* magnitudes that were derived from the GAIA and Pan-STARR catalogs and are "native" magnitudes of the catalog.

We used the ATLAS r′ (SR) magnitudes. Zero-point adjustments are mostly ≤ 0.03 mag. The occasions where larger corrections were required may have been related in part to using unfiltered observations, poor centroiding of the reference stars, and not correcting for second-order extinction terms.

The Y-axis values are ATLAS SR "sky" (catalog) magnitudes. The two values in the parentheses are the phase angle (a) and the value of *G* used to normalize the data to the comparison stars used in the earliest session. This, in effect, made all the observations seem to be made at a single fixed date/time and phase angle, leaving any variations due only to the asteroid's rotation and/or albedo changes. The X-axis shows rotational phase from –0.05 to 1.05. If the plot includes the amplitude, e.g., "Amp: 0.65", this is the amplitude of the Fourier model curve and *not necessarily the adopted amplitude for the lightcurve*.

For brevity, only some of the previously reported rotational periods may be referenced. A complete list is available at the asteroid lightcurve database (LCDB; Warner et al., 2009).

<u>1063 Aquilegia</u>. We observed this member of the Flora family/group once before (Stephens, 2018) finding a rotational period of 5.794 h. The result from this apparition is similar.

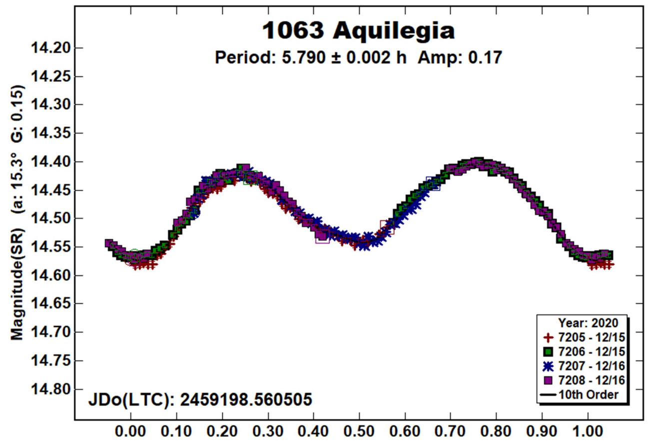

In addition to our dense data from the two apparitions, we used sparse data from the AstDyS-2 site and dense data from Waszczak et al. (2015) in the Asteroid Lightcurve Data Exchange Format database (ALCDEF, 2020), to solve for the sidereal period and pole position and create a shape model. These data were combined using *MPO LCInvert* (Bdw Publishing). This Windows-based program incorporates the algorithms developed by Kaasalainen and Torppa (2001) and Kaasalainen et al (2001) and converted by Josef Durech from the original FORTRAN to C. A period search was made over a sufficiently wide range to assure finding a global minimum in χ^2 values.

Our pole model showed two possible solutions 180° apart; (λ, β, *P*) = (46°, 26°, 5.791760 h) and (λ, β, *P*) = (231°, 33°, 5.791761 h). Our preferred solution is (46°, 26°). The full set of inversion graphics are given at the end of this paper.

<u>1570 Brunonia</u>. Using data from the Kepler Space Telescope, Molnár et al. (2018) previously reported a period > 45 h for this member of the Koronis family/group.

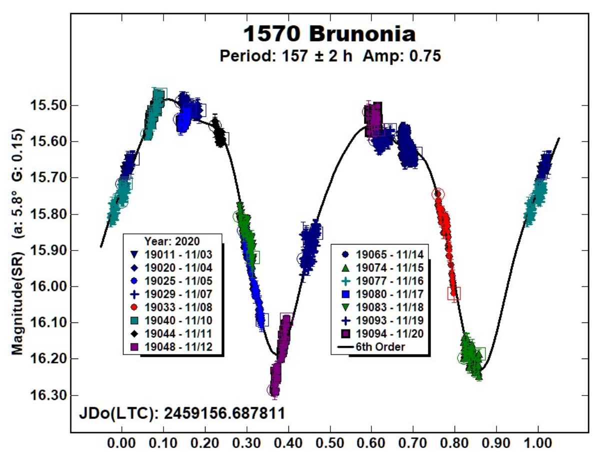

With observations spanning nearly three weeks, we were able to determine a period of 157 h. There is a hint of tumbling, which is probable given that the damping time period is about 137 h (Pravec et al., 2014; short damping times on F-D plot).

2254 Requiem. We have observed this member of the Flora family/group twice in the past (Stephens, 2018, 4.432 h; Warner, 2013, 4.430 h).

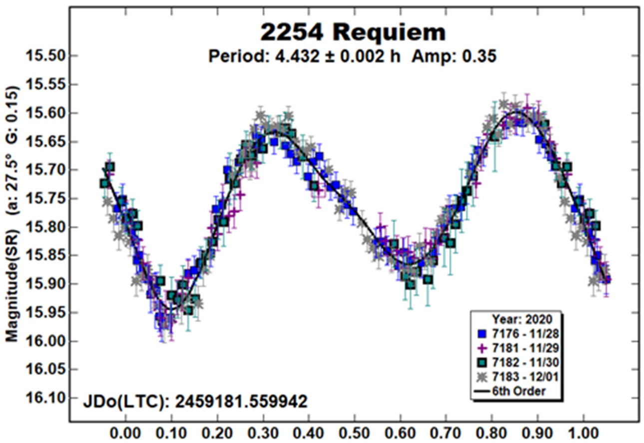

In addition to our dense data from four apparitions, we used sparse data from the AstDyS-2 site and dense data from Waszczak et al. (2015) in the ACLDEF database (ALCDEF, 2020), to solve for the sidereal period and pole position and create a shape model.

Our pole model showed two possible solutions 180° apart; (λ, β, *P*) = (38°, 48°, 4.430326 h) and (λ, β, *P*) = (223°, 38°, 4.430327 h). Our preferred solution is (223°, 38°). The full set of inversion graphics are given at the end of this paper.

2346 Lilio. This member of the Erigone family/group has four rotational periods reported by Behrend (2003web; 2005web; 2007web; 2016web). We observed it twice in the past (Warner, 2006; Stephens, 2016a). Each time the period was near 3.03 h.

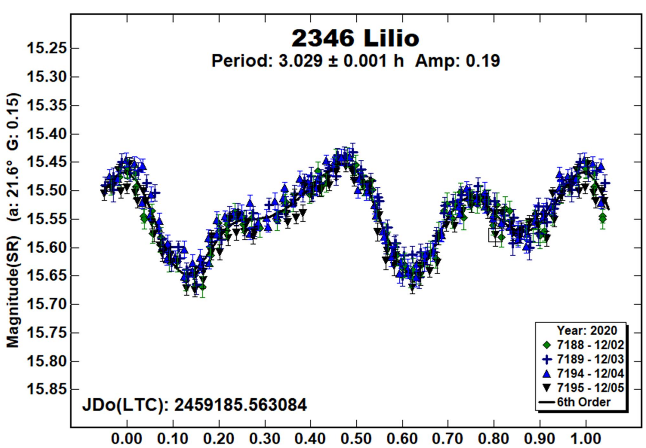

In addition to our dense data from four apparitions, we used sparse data from the AstDyS-2 site to solve for the sidereal period and pole position and create a shape model. We found two possible pole solutions 180° apart: (λ, β, *P*) = (164°, 5°, 3.029079 h) and (λ, β, *P*) = (349°, 19°, 3.029079 h). Our preferred solution is (164°, 5°). The full set of inversion graphics are given at the end of this paper.

2510 Shandong. This member of the Flora family/group observed twice in the past (Higgins and Goncalves, 2006, 5.9463 h; Stephens and Warner, 2019, 5.949 h). Hanuš et al. (2013) reported a spin axis model with (λ, β, *P*) = (256°, 27°) or (71°, 17°) and a sidereal period of 5.94639 h.

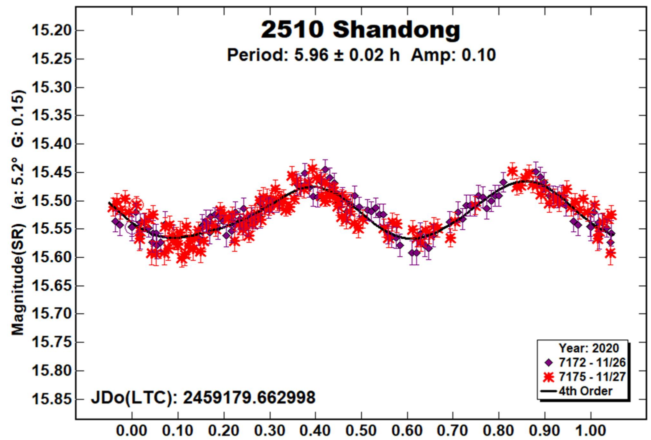

Because of the availability of the dense data from Higgins et al. in the ALCDEF database (ALCDEF, 2020), sparse data at the Asteroids - Dynamic web site (AstDyS-2, 2020), and our dense data from two apparitions, we attempted to solve for the sidereal period and pole position and create a shape model. A period search was made over a sufficiently wide range to assure finding a global minimum in χ^2 values.

Our pole model showed two possible solutions 180° apart and reversed the preference of the Hanuš et al. solution; (λ, β, *P*) = (80°, –45°, 5.947032 h) and (λ, β, *P*) = (250°, –35°, 5.947033 h). Our preferred solution is (80°, –45°). The addition of future dense and sparse datasets will eventually break the tie. The full set of inversion graphics are given at the end of this paper.

2912 Lapalma. This member of the Flora family was observed in 2008 by Brinsfield (2008, 5.71 h) and Pravec et al. (2008web, 5.71076 h). Our work this year is in good agreement.

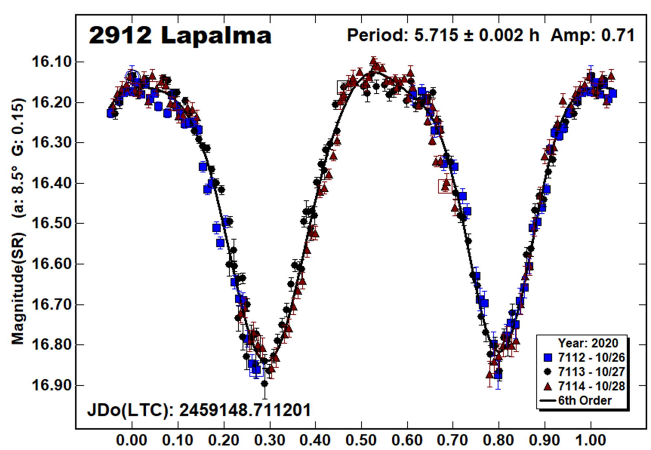

3781 Dufek. We could not find any entries in the LCDB for this member of the Koronis family/group. There are presently only five asteroids in the LCDB with a longer rotational period and U ≥ 2–. A general rule of thumb (Pravec et al., 2014) would have Dufek tumbling. There are no obvious signs of that.

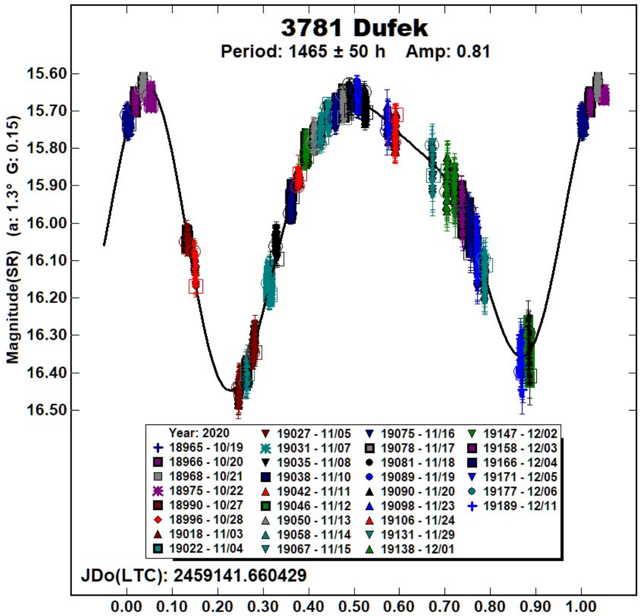

(20498) 1999 RT1. This member of the Eunomia family/group was a target of opportunity, being in the field of the Jovian Trojan, 3063 Makhaon for three nights. It was observed in 2019 May by Pál et al. (2020), using data from TESS. They reported a period of 14.4512 h, in good agreement with the results from this year.

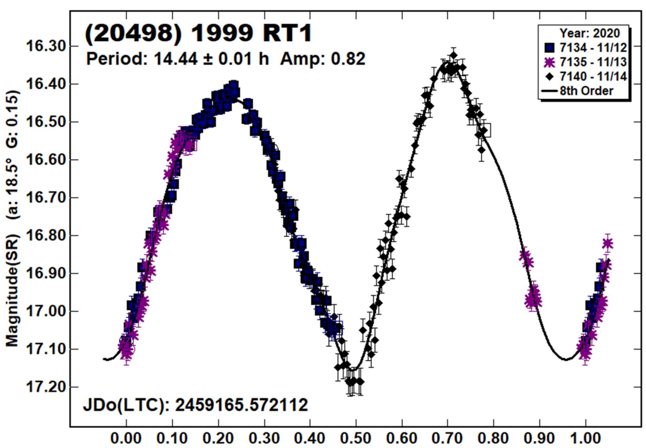

(21182) 1994 EC2. There are no previous rotational periods listed in the LCDB for this member of the Phocaea family/group.

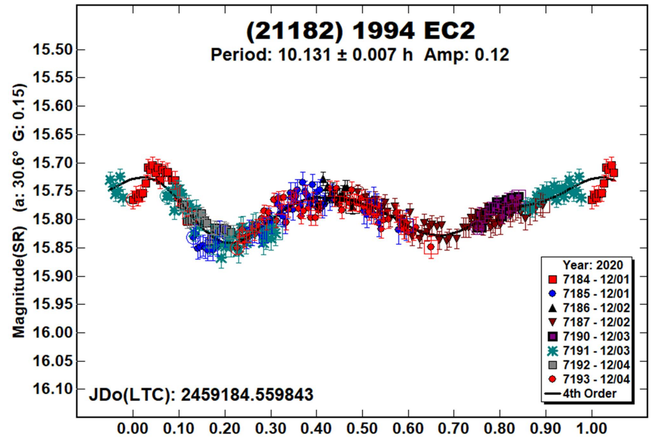

(32772) 1986 JL. We have observed this 4-km sized member of the Hungaria group/family three times in the past (Warner, 2013, 6.047 h; Stephens, 2016b, 6.049 h; Stephens and Warner, 2019, 6.046 h). The results this year are in good agreement, while having the lowest amplitude of all the apparitions.

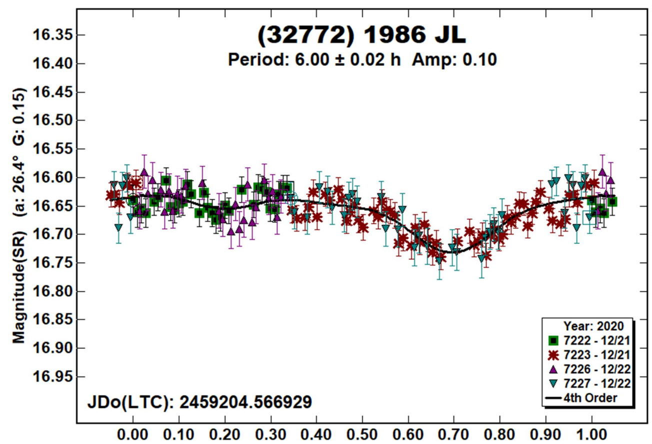

(69274) 1989 UZ1. There are no previous references in the LCDB for this 2.5-km Mars-crosser.

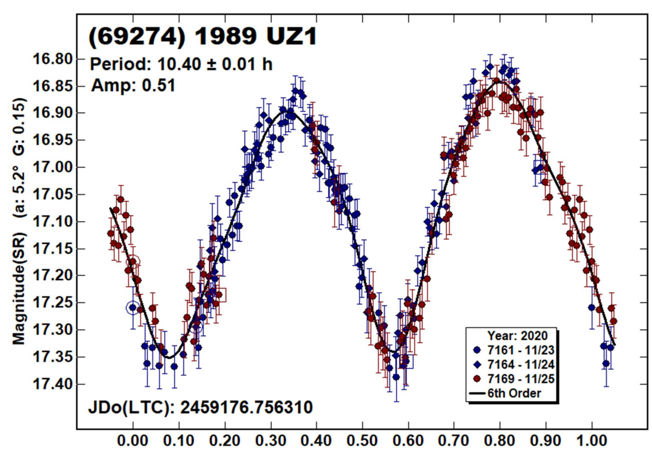

SPIN/SHAPE MODEL FOR 1063 Aquilegia

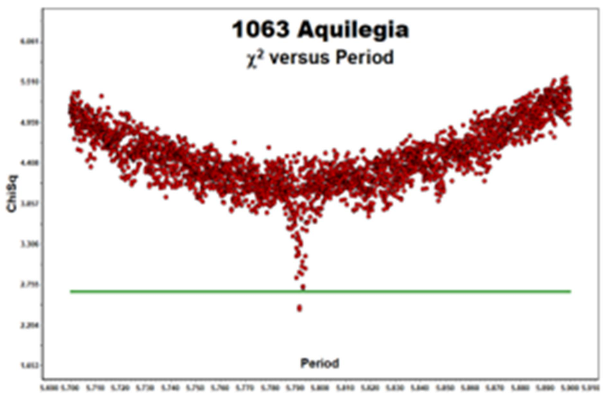

Figure 1. The initial period search results.

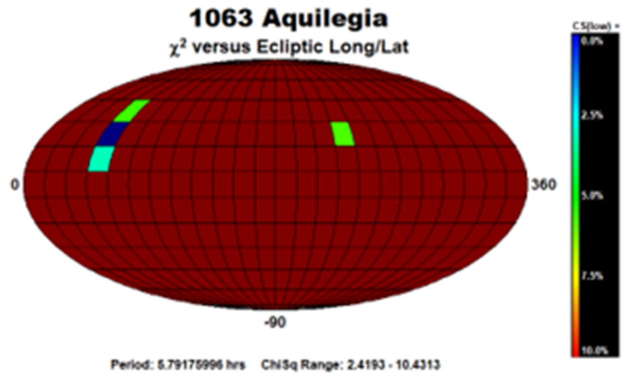

Figure 2. The pole search found two probable solutions.

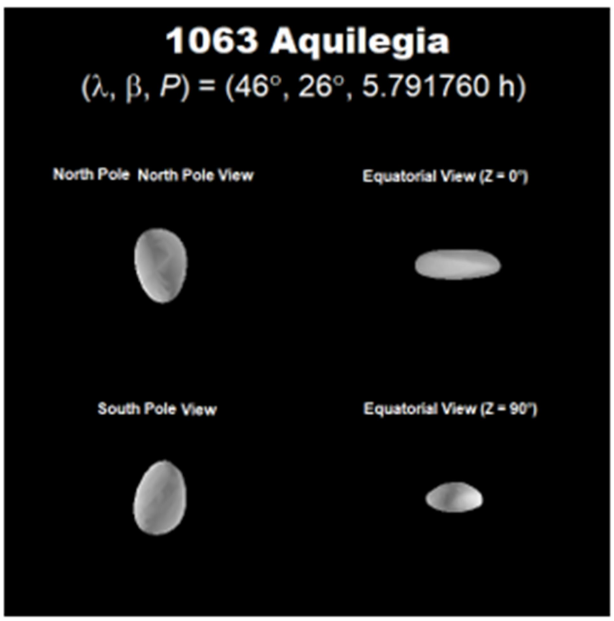

Figure 3. The shape of the asteroid based on the preferred solution.

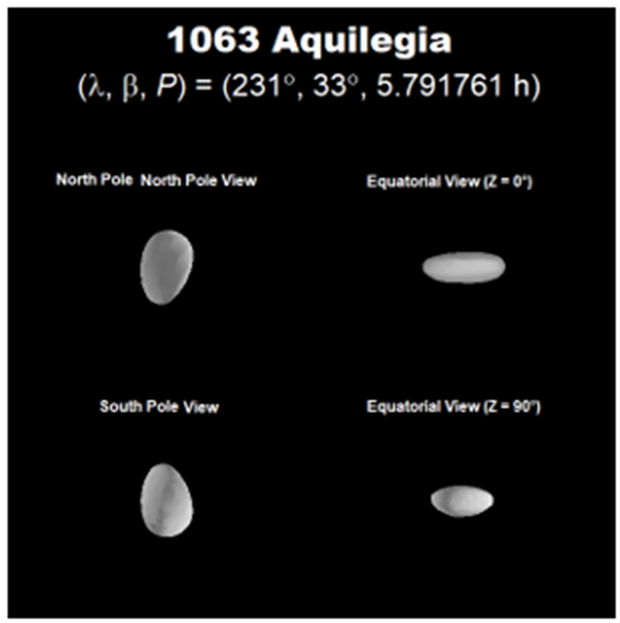

Figure 4. The shape of the asteroid based upon the secondary solution.

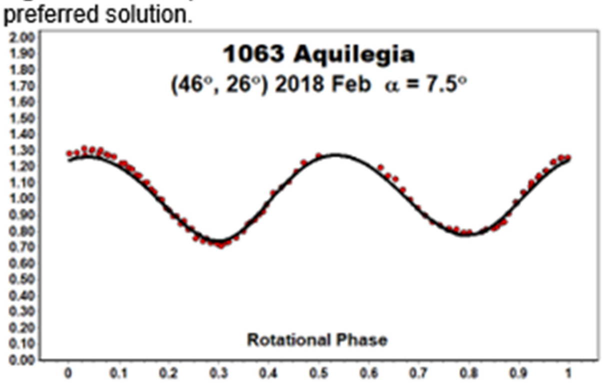

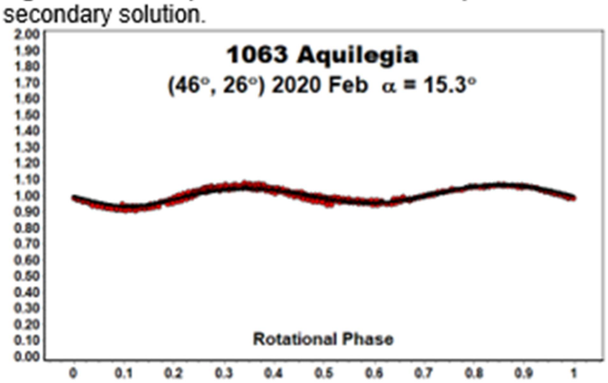

Figure 5/6. The comparison plots are against the preferred pole solution. The red dots indicate the data used for modeling while the black line is the smoothed lightcurve for generated by the shape at the time of the observations. The match is very close on both occasions, which gives confidence in the shape/spin axis model.

SPIN/SHAPE MODEL FOR 2254 Requiem

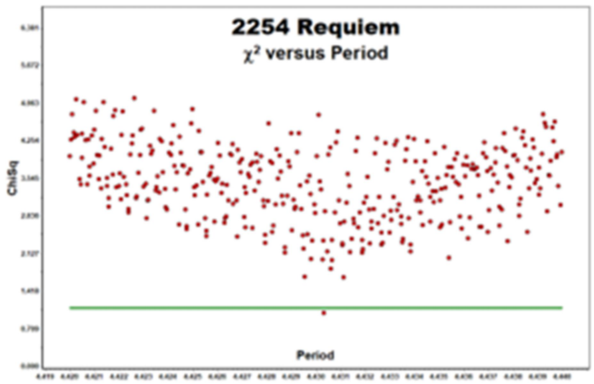

Figure 1. The initial period search results.

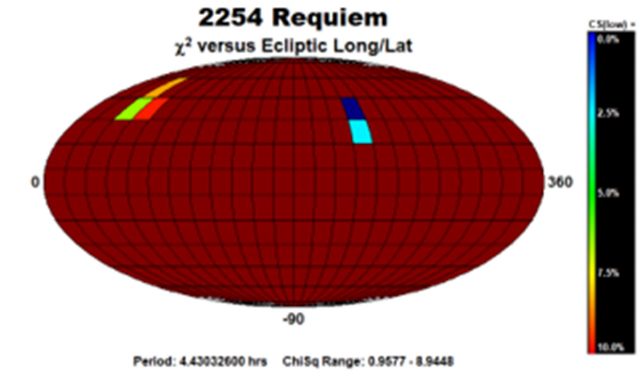

Figure 2. The pole search found two probable solutions.

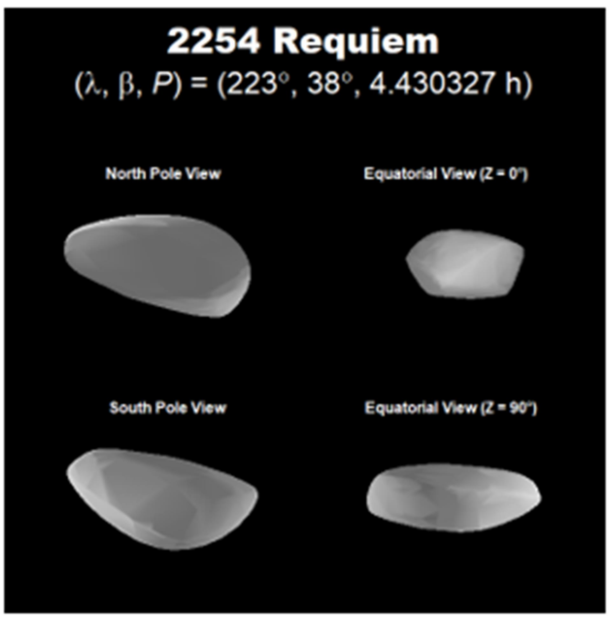

Figure 3. The shape of the asteroid based on the preferred solution.

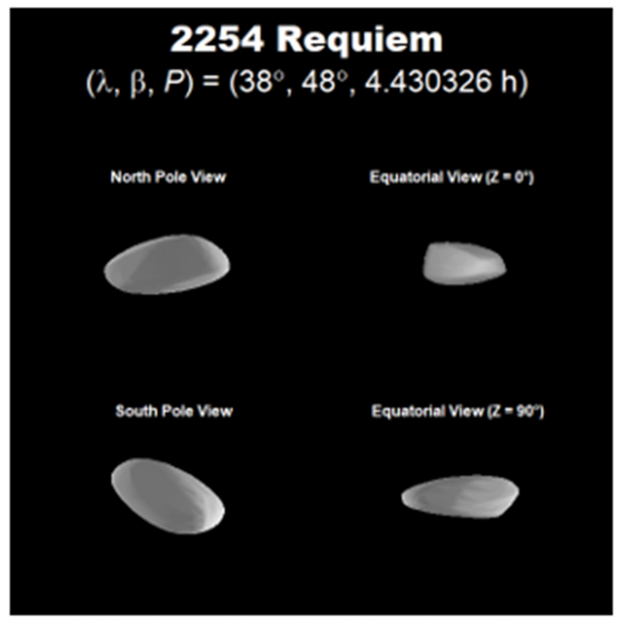

Figure 4. The shape of the asteroid based upon the secondary solution.

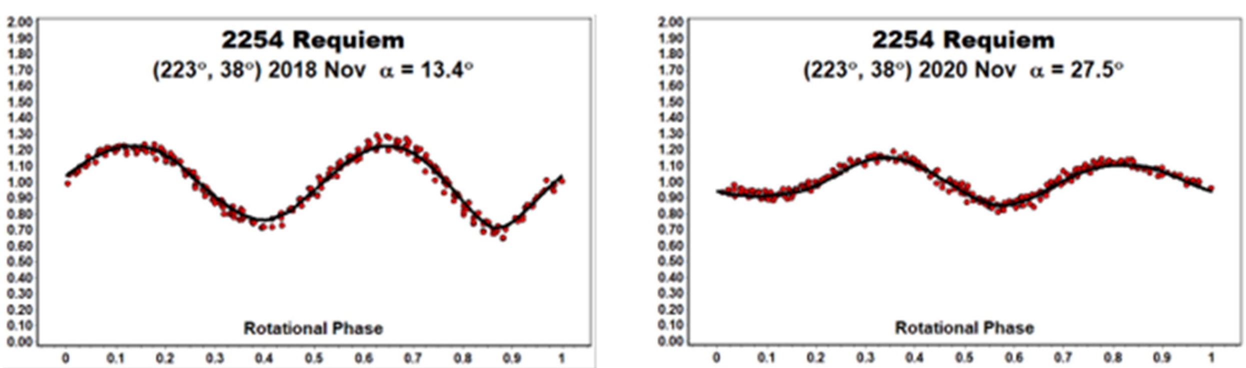

Figure 5/6. The comparison plots are against the preferred pole solution. The red dots indicate the data used for modeling while the black line is the smoothed lightcurve for generated by the shape at the time of the observations. The match is very close on both occasions, which gives confidence in the shape/spin axis model.

SPIN/SHAPE MODEL FOR 2346 LILIO

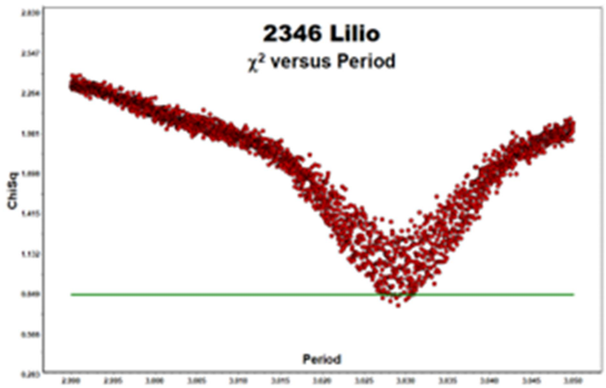

Figure 1. The initial period search results.

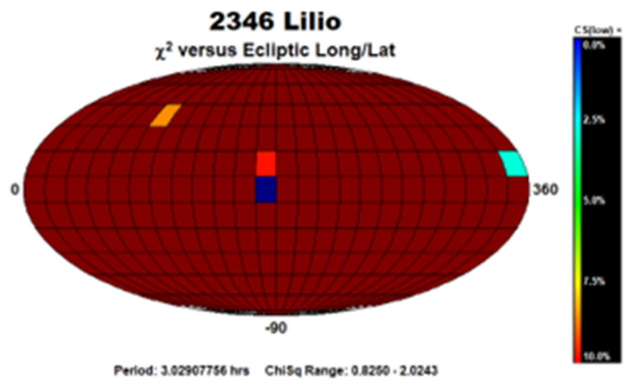

Figure 2. The pole search found two probable solutions.

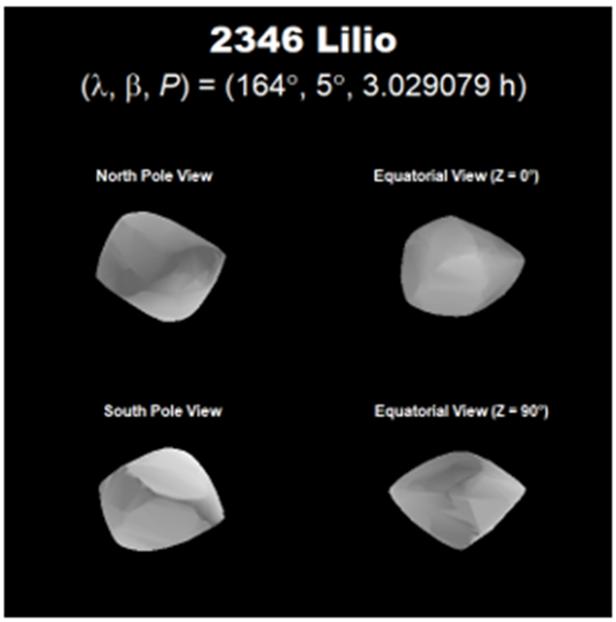

Figure 3. The shape of the asteroid based on the preferred solution.

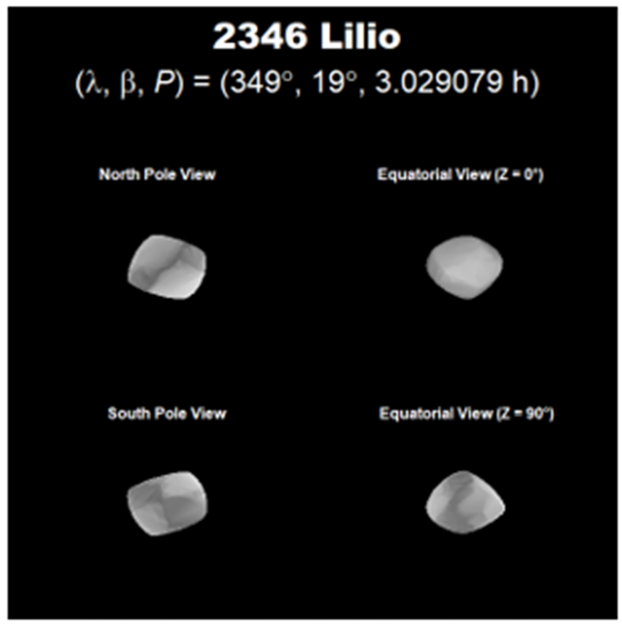

Figure 4. The shape of the asteroid based upon the secondary solution.

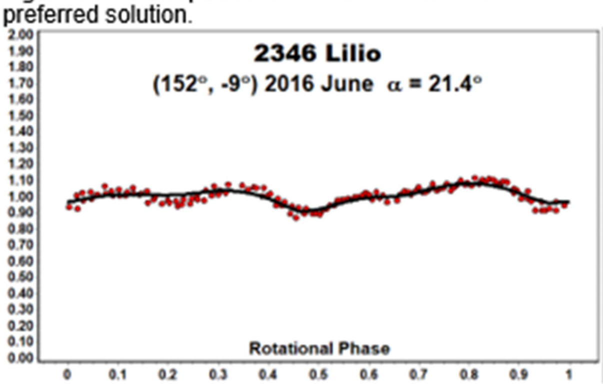

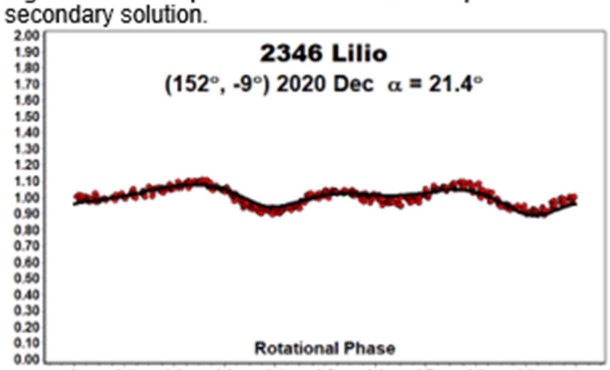

Figure 5/6. The comparison plots are against the preferred pole solution. The red dots indicate the data used for modeling while the black line is the smoothed lightcurve for generated by the shape at the time of the observations. The match is very close on both occasions, which gives confidence in the shape/spin axis model.

SPIN/SHAPE MODEL FOR 2510 Shandong

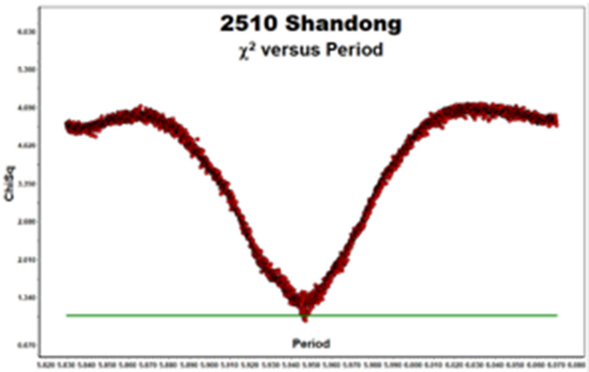

Figure 1. The initial period search results.

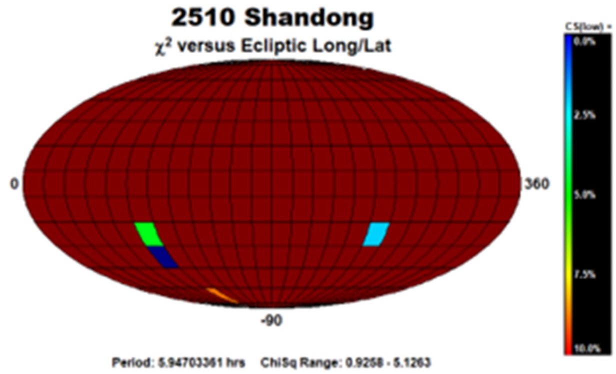

Figure 2. The pole search found two probable solutions.

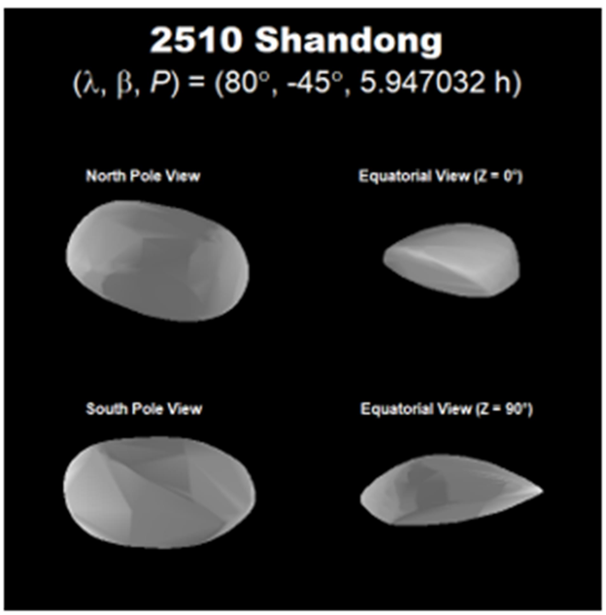

Figure 3. The shape of the asteroid based on the preferred solution.

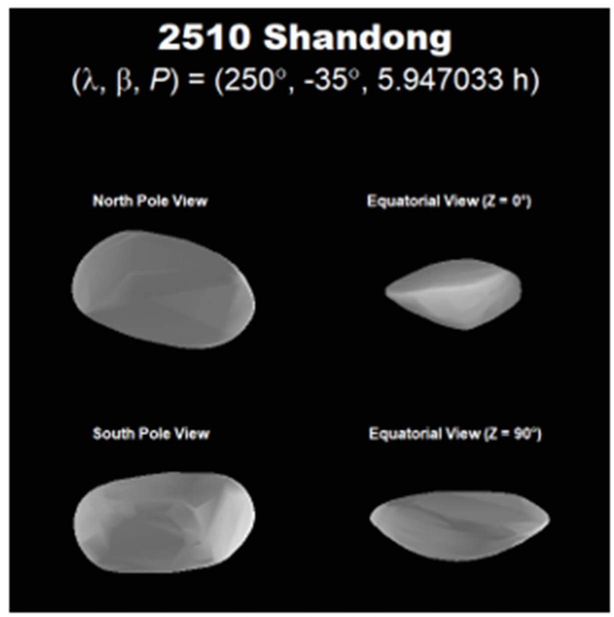

Figure 4. The shape of the asteroid based upon the secondary solution.

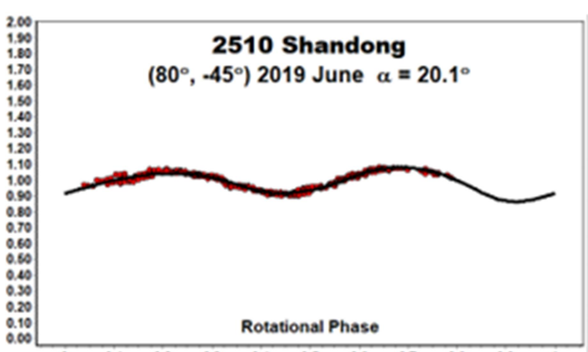

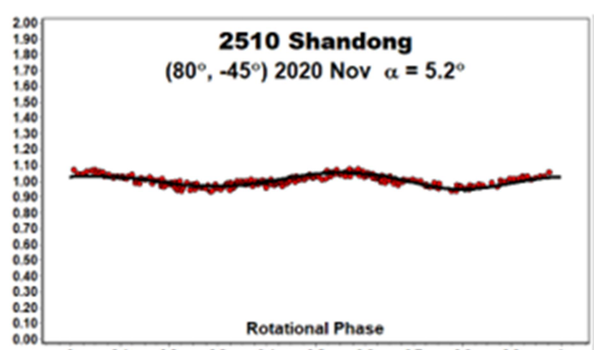

Figure 5/6. The comparison plots are against the preferred pole solution. The red dots indicate the data used for modeling while the black line is the smoothed lightcurve for generated by the shape at the time of the observations. The match is very close on both occasions, which gives confidence in the shape/spin axis model.

Number	Name	2020 mm/dd	Phase	L_{PAB}	B_{PAB}	Period(h)	P.E.	Amp	A.E.	Grp
1063	Aquilegia	12/15-12/16	15.4,15.7	51	-5	5.790	0.002	0.17	0.01	FLOR
	Pole (λ, β, P)	**(46°, 26°, 5.791760 h)**	(231°, 33°, 5.791761 h)				**a/b: 1.84**	**a/c: 2.49**		
1570	Brunonia	11/03-11/20	5.9,12.4	28	-1	157	2	0.8	0.05	KOR
2254	Requiem	11/28-12/01	27.6,27.9	10	4	4.432	0.002	0.35	0.02	FLOR
	Pole (λ, β, P)	**(223°, 38°, 4.430327 h)**	(38°, 48°, 4.430326 h)				**a/b: 1.67**	**a/c: 2.27**		
2346	Lilio	12/02-12/05	21.6,22.4	30	3	3.029	0.001	0.19	0.02	ERI
	Pole (λ, β, P)	**(164°, 5°, 3.029079 h)**	(349°, 19°, 3.029079 h)				**a/b: 1.26**	**a/c: 1.30**		
2510	Shandong	11/26-11/27	16.6,4.7	86	-2	5.96	0.02	0.1	0.01	FLOR
	Pole (λ, β, P)	**(80°, -45°, 5.947032 h)**	(250°, -35°, 5.947033 h)				**a/b: 1.32**	**a/c: 2.27**		
2912	Lapalma	10/26-10/28	8.5,7.7	47	-9	5.715	0.002	0.71	0.02	FLOR
3781	Dufek	10/19-12/12	*1.3,17.8	30	-1	1465	50	0.82	0.03	KOR
20498	1999 RT1	11/12-11/14	18.5,19.2	17	12	14.44	0.01	0.82	0.03	EUN
21182	1994 EC2	12/01-12/04	30.7,31.4	25	17	10.131	0.007	0.12	0.02	PHO
32772	1986 JL	12/21-12/22	26.5,26.8	47	-6	6.00	0.02	0.10	0.02	H
69274	1989 UZ1	11/23-11/25	5.2,4.0	68	-2	10.40	0.01	0.51	0.02	MC
306517	1999 WY	09/30-10/10	34.5,35.9	353	41	14.807	0.004	0.32	0.03	MC

Table II. Observing circumstances and results. The phase angle is given for the first and last date. If preceded by an asterisk, the phase angle reached an extrema during the period. L_{PAB} and B_{PAB} are the approximate phase angle bisector longitude/latitude at mid-date range (see Harris et al., 1984). Grp is the asteroid family/group (Warner et al., 2009): ERI, Erigone; EUN, Eunomia; FLOR, Flora; H, Hungaria; KOR, Koronis; MC, Mars-crosser; PHO, Phocaea. For 1063, 2254, 2346, and 2510, the second line gives the spin axis/shape modeling results. The preferred solution is in bold text.

(306517) 1999 WY. We could not find any entries in the LCDB for this Mars-crosser.

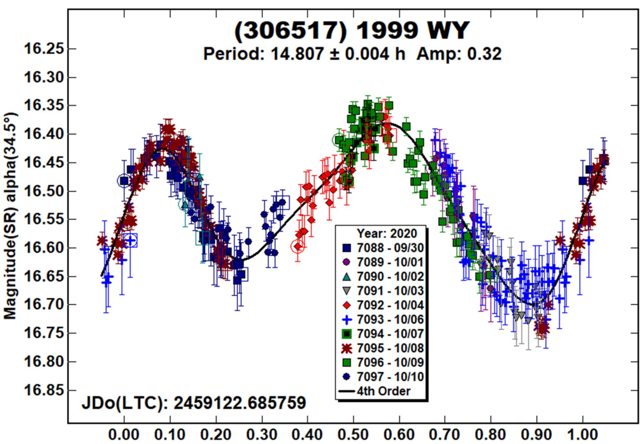

Acknowledgements

Observations at CS3 and continued support of the asteroid lightcurve database (LCDB; Warner et al., 2009) are supported by NASA grant 80NSSC18K0851.

This work includes data from the Asteroid Terrestrial-impact Last Alert System (ATLAS) project. ATLAS is primarily funded to search for near earth asteroids through NASA grants NN12AR55G, 80NSSC18K0284, and 80NSSC18K1575; byproducts of the NEO search include images and catalogs from the survey area. The ATLAS science products have been made possible through the contributions of the University of Hawaii Institute for Astronomy, the Queen's University Belfast, the Space Telescope Science Institute, and the South African Astronomical Observatory.

The authors gratefully acknowledge Shoemaker NEO Grants from the Planetary Society (2007, 2013). These were used to purchase some of the telescopes and CCD cameras used in this research.

References

AstDys-2 (2020). Asteroids - Dynamic site. *https://newton.spacedys.com/astdys/*

Asteroid Lightcurve Data Exchange Format database (ALCDEF). *http://www.alcdef.org/*

Behrend, R., (2003web, 2005web, 2007web, 2016web). Observatoire de Geneve web site. *http://obswww.unige.ch/~behrend/page_cou.html*

Brinsfield, J.W. (2008). "Asteroid Lightcurve Analysis at the Via Capote Observatory: First Quarter 2008." *Minor Planet Bul.* **35**, 119-122.

Hanuš, J.; Ďurech, J.; Brož, M.; Marciniak, A.; Warner, B.D.; Pilcher, F.; Stephens, R.; Behrend, R.; Carry, B.; and 111 coauthors. (2013). "Asteroids' physical models from combined dense and sparse photometry and scaling of the YORP effect by the observed obliquity distribution." *Astron. Astrophys.* **551**, A67.

Harris, A.W.; Young, J.W.; Scaltriti, F.; Zappala, V. (1984). "Lightcurves and phase relations of the asteroids 82 Alkmene and 444 Gyptis." *Icarus* **57**, 251-258.

Harris, A.W.; Young, J.W.; Bowell, E.; Martin, L.J.; Millis, R.L.; Poutanen, M.; Scaltriti, F.; Zappala, V.; Schober, H.J.; Debehogne, H.; Zeigler, K.W. (1989). "Photoelectric Observations of Asteroids 3, 24, 60, 261, and 863." *Icarus* **77**, 171-186.

Higgins, D.; Goncalves, R. (2006). "Asteroid Lightcurve Analysis at Hunters Hill Observatory and Collaborating Stations - June-September 2006." *Minor Planet Bull*. **34**, 16-18.

Kaasalainen, M.; Torppa J. (2001). "Optimization Methods for Asteroid Lightcurve Inversion. I. Shape Determination." *Icarus* **153**, 24-36.

Kaasalainen, M.; Torppa J.; Muinonen, K. (2001). "Optimization Methods for Asteroid Lightcurve Inversion. II. The Complete Inverse Problem." *Icarus* **153**, 37-51

Molnár, L.; Pál, A.; Sáneczky, K.; Szabó, R.; Vinkó, J.; Szabó, Gy.M.; Kiss, Cs.; Hanyecz, O.; Marton, G.; Kiss, L.L. (2018) "Main-belt Asteroids in the K2 Uranus Field." *Ap. J. Supp. Ser.* **234,** A37

Pál, A.; Szakáts, R.; Kiss, C.; Bódi, A.; Bognár, Z.; Kalup, C.; Kiss, L.L.; Marton, G.; Molnár, L.; Plachy, E.; Sárneczky, K.; Szabó, G.M.; Szabó, R. (2020). "Solar System Objects Observed with TESS - First Data Release: Bright Main-belt and Trojan Asteroids from the Southern Survey." *Ap. J.* **247**, A26.

Pravec, P.; Wolf, M.; Sarounova, L. (2008web). *http://www.asu.cas.cz/~ppravec/neo.htm*

Pravec, P.; Scheirich, P.; Durech, J.; Pollock, J.; Kusnirak, P.; Hornoch, K.; Galad, A.; Vokrouhlicky, D.; Harris, A.W.; Jehin, E.; Manfroid, J.; Opitom, C.; Gillon, M.; Colas, F.; Oey, J.; Vrastil, J.; Reichart, D.; Ivarsen, K.; Haislip, J.; LaCluyze, A. (2014). "The tumbling state of (99942) Apophis." *Icarus* **233**, 48-60.

Stephens, R.D. (2016a). "Asteroids Observed from CS3: 2016 January-March." *Minor Planet Bull*. **43**, 252-255.

Stephens, R.D. (2016b). "Asteroids Observed from CS3: 2016 April - June." *Minor Planet Bull*. **43**, 336-339.

Stephens, R.D. (2018). "Asteroids Observed from CS3: 2018 January - March." *Minor Planet Bull*. **45**, 299-301.

Stephens, R.D.; Warner, B.D. (2019). "Main-belt Asteroids Observed from CS3: 2019 April to June." *Minor Planet Bull*. **46**, 449-456.

Tonry, J.L.; Denneau, L.; Flewelling, H.; Heinze, A.N.; Onken, C.A.; Smartt, S.J.; Stalder, B.; Weiland, H.J.; Wolf, C. (2018). "The ATLAS All-Sky Stellar Reference Catalog." *Astrophys. J.* **867**, A105.

Warner, B.D. (2006). "Asteroid lightcurve analysis at the Palmer Divide Observatory: July-September 2005." *Minor Planet Bull.* **33**, 35-39.

Warner, B.D.; Harris, A.W.; Pravec, P. (2009). "The Asteroid Lightcurve Database." *Icarus* **202**, 134-146. Updated 2020 Oct. *http://www.minorplanet.info/lightcurvedatabase.html*

Warner, B.D. (2013). "Asteroid Lightcurve Analysis at the Palmer Divide Observatory: 2013 January - March." *Minor Planet Bull.* **40**, 137-145.

Waszczak, A.; Chang, C.-K.; Ofek, E.O.; Laher, R.; Masci, F.; Levitan, D.; Surace, J.; Cheng, Y.-C.; Ip, W.-H.; Kinoshita, D.; Helou, G.; Prince, T.A.; Kulkarni, S. (2015). "Asteroid Light Curves from the Palomar Transient Factory Survey: Rotation Periods and Phase Functions from Sparse Photometry." *Astron. J.* **150**, A75.

PERIOD DETERMINATIONS FOR SEVENTEEN MINOR PLANETS

Tom Polakis
Command Module Observatory
121 W. Alameda Dr.
Tempe, AZ 85282
tpolakis@cox.net

(Received: 2020 Dec 28)

Phased lightcurves and synodic rotation periods for 17 main-belt asteroids are presented, based on CCD observations made from 2020 October through 2020 December. All the data have been submitted to the ALCDEF database.

CCD photometric observations of 17 main-belt asteroids were performed at Command Module Observatory (MPC V02) in Tempe, AZ. Images were taken using a 0.32-m f/6.7 Modified Dall-Kirkham telescope, SBIG STXL-6303 CCD camera, and a 'clear' glass filter. Exposure time for all the images was 2 minutes. The image scale after 2×2 binning was 1.76 arcsec/pixel. Table I shows the observing circumstances and results. All of the images for these asteroids were obtained between 2020 October and 2020 December.

Images were calibrated using a dozen bias, dark, and flat frames. Flat-field images were made using an electroluminescent panel. Image calibration and alignment was performed using MaxIm DL software.

The data reduction and period analysis were done using MPO Canopus (Warner, 2020). The 45′×30′ field of the CCD typically enables the use of the same field center for three consecutive nights. In these fields, the asteroid and three to five comparison stars were measured. Comparison stars were selected with colors within the range of $0.5 < B-V < 0.95$ to correspond with color ranges of asteroids. In order to reduce the internal scatter in the data, the brightest stars of appropriate color that had peak ADU counts below the range where chip response becomes nonlinear were selected. MPO Canopus plots instrumental vs. catalog magnitudes for solar-colored stars, which is useful for selecting comp stars of suitable color and brightness.

Since the sensitivity of the KAF-6303 chip peaks in the red, the clear-filtered images were reduced to Sloan r′ to minimize error with respect to a color term. Comparison star magnitudes were obtained from the ATLAS catalog (Tonry et al., 2018), which is incorporated directly into MPO Canopus. The ATLAS catalog derives Sloan griz magnitudes using a number of available catalogs. The consistency of the ATLAS comp star magnitudes and color-indices allowed the separate nightly runs to be linked often with no zero-point offset required or shifts of only a few hundredths of a magnitude in a series.

A 9-pixel (16 arcsec) diameter measuring aperture was used for asteroids and comp stars. It was typically necessary to employ star subtraction to remove contamination by field stars. For the asteroids described here, I note the RMS scatter on the phased lightcurves, which gives an indication of the overall data quality including errors from the calibration of the frames, measurement of the comp stars, the asteroid itself, and the period-fit. Period determination was done using the MPO Canopus Fourier-type FALC fitting method (cf. Harris et al., 1989). Phased lightcurves show the maximum at phase zero. Magnitudes in these plots are apparent and scaled by MPO Canopus to the first night.